Atmospheric Environment 309 (2023) 119917

Contents lists available at ScienceDirect

Atmospheric Environment

journal homepage: www.elsevier.com/locate/atmosenv

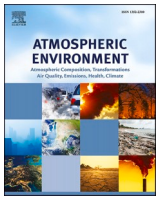

Biogenic volatile organic compounds enhance ozone production and complicate control efforts: Insights from long-term observations in Hong Kong

Yingnan Zhang [a,b,1], Jianing Dai [a,c,1], Qinyi Li [a], Tianshu Chen [a], Jiangshan Mu [b], Guy Brasseur [c], Tao Wang [a,*], Likun Xue [b,**]

[a] Department of Civil and Environmental Engineering, The Hong Kong Polytechnic University, Hong Kong, China
[b] Environment Research Institute, Shandong University, Qingdao, China
[c] Environmental Modeling Group, Max Planck Institute for Meteorology, Hamburg, Germany

HIGHLIGHTS

- Measurements of O_3 and its precursors in Hong Kong during 2013–2019 were analyzed.
- Driven by the warming temperature, isoprene at Tung Chung increased by 18%/yr.
- Increased BVOCs enhanced O_3 production and affected the O_3-NO_x-AVOCs relationship.

ARTICLE INFO

Keywords:
Biogenic VOCs
O_3 pollution
Control efforts
Long-term observations
MCM box model

ABSTRACT

Ground-level ozone (O_3) pollution is a major air-quality issue in China. With decreasing emissions of anthropogenic precursors, natural precursors may become increasingly important in O_3 pollution. However, understanding of the change in biogenic volatile organic compounds (BVOCs) and its environmental impact in China has been hindered by the lack of long-term measurements of VOCs. In this study, we analyze the continuous measurements of O_3 and its precursors obtained in Hong Kong during 2013–2019 and demonstrate the increasingly important role of BVOCs in O_3 production. Driven by the warming temperature, Biogenic isoprene at a suburban site (Tung Chung) increased by 0.05 ± 0.02 ppbv/yr (18%/yr), which is in sharp contrast to the decreases in anthropogenic precursors during the study period. Detailed chemical modeling shows that increased BVOCs enhanced local O_3 production by 0.31 ppbv/h/yr (23%) annually, and the effect was the most obvious in summer (by 0.44 ppbv/h/yr or 27%). Increased BVOCs also affected the O_3-precursor (anthropogenic) relationships by increasing the O_3 sensitivity to nitrogen oxides (NO_x) and decreasing the O_3 sensitivity to anthropogenic VOCs (AVOCs). Despite changes in precursors (decreasing NO_x, increasing BVOCs, and decreasing some AVOCs), the O_3 formation remains in VOC-limited regimes at Tung Chung. Joint control of AVOCs and NO_x (at a ratio greater than 1.2) would help avoid exacerbation of O_3 pollution and reduce NO_2 pollution. In the short term, an AVOCs-focused strategy would help reduce O_3 to a moderate level; but because of the presence of the natural BVOCs, a drastic cut in NO_x emissions would be needed to meet a more stringent O_3 standard. Our findings also suggest the BVOCs increase likely occurred in the larger Pearl River Delta (PRD) region, and thus the results from our study in Hong Kong may have implications for developing AVOCs/NO_x reduction measures in the PRD region and beyond.

* Corresponding author.
** Corresponding author.
E-mail addresses: cetwang@polyu.edu.hk (T. Wang), xuelikun@sdu.edu.cn (L. Xue).
[1] These authors contributed equally.

https://doi.org/10.1016/j.atmosenv.2023.119917
Received 9 April 2023; Received in revised form 13 June 2023; Accepted 19 June 2023
Available online 28 June 2023

1. Introduction

Tropospheric ozone (O_3) is a key component of photochemical smog and would adversely affect human health, vegetation growth, and climate change (Agathokleous et al., 2020; Fleming et al., 2018; Gaudel et al., 2018; Lefohn et al., 2018; Mills et al., 2018). Since the first discovery in Los Angeles in the 1950s, O_3 pollution has evolved into a major air quality issue faced by many of the world's urban and industrialized regions (Zhang et al., 2019), including many parts of China (Sun et al., 2016, 2019; Wang et al., 2022). As a typical secondary pollutant, O_3 is mainly formed via photochemical reactions involving carbon monoxide (CO), nitrogen oxides (NO_x), and volatile organic compounds (VOCs) (Wang et al., 2017a). In the polluted regions, CO and NO_x mainly originate from anthropogenic emissions, while the level of VOCs is subject to the influence of both anthropogenic emissions (i.e., AVOCs) and biogenic emissions (i.e., BVOCs) (Guo et al., 2017). Understanding the change in precursors of different origins and its underlying impact on O_3 production is of great importance for the mitigation of O_3 pollution.

Hong Kong is located in the Guangdong-Hongkong-Macao Greater Bay Area, one of the major city clusters and O_3 pollution hotspots in China (Wang et al., 2022). It is a highly urbanized megacity with high vegetation coverage (~78% according to Hong Kong Development Bureau). To alleviate O_3 pollution, the government has devoted substantial efforts to control anthropogenic precursors, e.g., phase out of diesel commercial vehicles, regulation of solvent usage, and replacement of catalytic converters on liquified petroleum gas-fueled vehicles (https://www.epd.gov.hk/). These control measures have largely reduced the ambient concentrations of most air pollutants, but the O_3 levels remain high relative to the air quality objective of Hong Kong in both urban (e.g., Zeren et al., 2022) and nonurban (Wang et al. (2019) areas. By analyzing the city-wide O_3 concentration data obtained from the regular air quality network and the continuous measurements of VOCs at a suburban site (Tung Chung, TC) in western Hong Kong, Xue et al. (2014) showed that the increasing outside transport negated local efforts, leading to the overall upward trend of maximum daily 8 h average (MDA8) O_3 concentrations in Hong Kong in the O_3-peak autumn season from 2002 to 2013. Wang et al. (2019) showed leveling-off ozone concentrations at a coastal background site in mainland-originating air mass but increasing contributions from the air mass from Southeast Asia (mainly occurring in summer). Zeren et al. (2022) analyzed the data from the above-mentioned suburban site, and their result indicated that the MDA8 O_3 concentrations at TC stabilized from 2013 to 2017 as a combined result of decreasing regionally-transported O_3 and increasing locally-produced O_3. It remains unclear how the changes in the O_3 precursors in recent years have affected the local O_3 production in Hong Kong, especially regarding the role of BVOCs amid of rising surface temperatures (https://www.hko.gov.hk/).

In this study, we analyzed the measurement data of O_3 and its precursors in Hong Kong during 2013–2019, with the aim to quantify the effects of the changes in NO_x, anthropogenic VOCs, and BVOCs on surface O_3. We show that increasing BVOC concentrations are an important driver of elevated O_3 concentrations at Tung Chung alongside decreasing NO_x concentrations. We elucidate the mechanism by which increased BVOCs affect the O_3-NO_x-AVOCs relationships and the control efforts against O_3 pollution. We also discuss the implications of this study in Hong Kong for the control of O_3 pollution in other metropolitan areas.

2. Materials and methods

2.1. Measurement data

The measurement data during 2013–2019 were analyzed to examine the recent change in O_3 and its precursors in Hong Kong. The hourly measurements of O_3, CO, NO, and NO_x* (=NO + NO_2*) were obtained from 11 Air Quality Monitoring Stations (AQMSs) operated by the Hong Kong Environmental Protection Department (HKEPD) (see Fig. 1 and Table S1 for the location and data availability at each AQMS). These 11 AQMSs are located in residential areas or mixed functional areas (e.g., residential-commercial-industrial areas) and can well reflect the ambient level of air pollution that people are exposed to most of the time. The species were routinely monitored by commercial instruments (EPD, 2013-2019). Briefly, O_3 was measured by a UV photometric ozone analyzer, NO-NO_2-NO_x was measured using a chemiluminescence analyzer with NO_2 being converted to NO by molybdenum oxide (MoO), and CO was measured by a gas filter correlation, non-dispersive infrared analyzer. Details about quality assurance and quality control procedures for these species have been documented in previous studies (Wang et al., 2017b; Zeren et al., 2022). The MoO method is known to cause positive bias for NO_2 measurements as it converts not only NO_2 but also other oxidized nitrogen such as nitrous acid (HONO), peroxyacetyl nitrate (PAN), and nitric acid (HNO_3) (e.g., Xu et al., 2013). We denote the NO_2 measured by the MoO method as NO_2*.

We made use of the hourly observations of VOCs and other regular air pollutants at TC station, one of the above 11 AQMSs, for detailed modeling of the contributions of different precursors to O_3 production at the site. The TC station is located in a residential area of a new town (Tung Chung) in western Hong Kong. The Hong Kong International Airport is located to the north of the station at a distance of 3 km, and the nearby mountainous areas are covered with mixed vegetation. The TC area has been known to be a hot spot of O_3 pollution in Hong Kong (e.g., Xue et al., 2014; EPD, 2013-2019, see also Fig. S1). Non-methane hydrocarbons (NMHCs) were measured in real-time by two commercial GC-FID analyzers (Syntech Spectras GC 955, Series 600 and 800) with one for C_2–C_5 hydrocarbons (Series 600) and the other for C_6–C_{12} hydrocarbons (Series 800). Totally, 30 VOC species (covering 11 alkanes, 9 alkenes, 9 aromatics, and 1 alkyne) were detected with a detection limit ranging from 0.002 to 0.056 ppbv. Calibrations were performed on a weekly basis by using standard gases and built-in computerized programs. Details about the quality assurance and quality control procedures for VOCs measurement have been described in previous studies (Wang et al., 2017b; Zeren et al., 2022).

The hourly measurements of various meteorological parameters (e.g., temperature, relative humidity (RH), pressure, solar radiation, and wind direction and speed) were obtained from Hong Kong Observatory's King's Park (KP) station (see Fig. 1 for its location). The meteorological data are used as input to quantify changes in the local meteorological conditions on the O_3 production at the TC station.

In addition, we analyzed the hourly measurements at Hok Tsui, a background site in Hong Kong, during 2013–2019 to show the trends in background O_3 levels in Hong Kong (Wang et al., 2019). The vertical column of formaldehyde (HCHO) data, retrieved from the Ozone Monitoring Instruments (OMI) products, in autumn 2013 and 2019 were analyzed to track the variations in VOC abundance in the Pearl River Delta (PRD) region. The data on the annual average temperature in the PRD region were derived from the Guangdong Statistical Yearbook.

2.2. MCM chemical box model

A chemical box model was adopted to investigate the effect of changes in biogenic precursors and anthropogenic precursors on the detailed mechanisms of O_3 production. The chemical box model was run on the platform of framework for 0-D atmospheric modelling (F0AM) (Wolfe et al., 2016). It is built on the near-explicit chemical mechanism of Master Chemical Mechanism (MCM v3.3.1), which describes the chemical degradation of 143 primary VOC species in detail (Jenkin et al., 2003, 2015; Saunders et al., 2003). In addition, the model incorporates physical processes such as solar radiation, dry deposition, planetary boundary layer evolution, and dilution with background air (Zhang et al., 2021a, 2021b). Totally, three sets of simulations were performed with the application of the MCM chemical box model, i.e.,

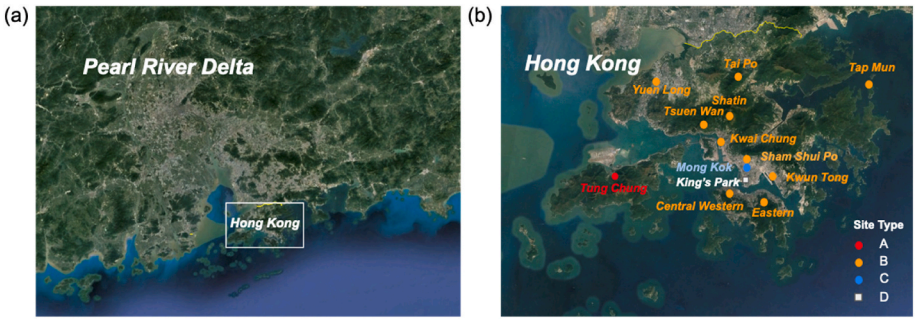

Fig. 1. (a) Map showing the location of Hong Kong and the adjacent Pearl River Delta region. (b) Map showing the 12 air quality monitoring stations (AQMSs) and one weather station in Hong Kong whose measurements were used in the present study. Types A and B represent Tung Chung station and the other 10 general stations, respectively; Types C and D represent the roadside station of Mong Kok and the weather station of King's Park, respectively. The maps are from Google Earth.

base model simulation, sensitivity test, and empirical kinetics modeling approach (EKMA). Details about the model scenarios are provided in Table S2, and are summarized below.

The base model simulation was performed to calculate the in-situ O_3 production rates at TC during 2013–2019. Briefly, the model was constrained by the seasonal-average diurnal profiles of NO, NO_2, HONO, O_3, SO_2, CO, CH_4, C_2–C_{10} NMHCs, temperature, RH, and the photolysis frequency of NO_2 (JNO_2), which were averaged or interpolated into a 1-h time resolution. The input of NO_2 was obtained by adjusting the NO_2* data at the TC station according to the average NO_2*/NO_2 ratios measured at the same site by Xu et al. (2013) (See SI for details). To obtain a more reliable modeling result, the OVOCs were initialized according to observation data. JNO_2 and HONO were not continuously measured over the study period. The corresponding model inputs were processed as follows. JNO_2 was estimated according to its linear regression relationship with solar radiation, and the relationship was determined based on an intensive field campaign at a supersite station in Hong Kong (Xia et al., 2022). HONO was constrained by the seasonal-average diurnal profile measured during 2011-2012 (Xu et al., 2015) and assumed constant during 2013–2019. We conducted sensitivity tests to evaluate the uncertainty introduced by the HONO treatment, see SI for details. The model was initiated at 00:00 local time (LT) and read the input data at an integration step of 1 h to calculate in-situ O_3 production, destruction, and net rates (see SI for the calculation). Prior to each simulation, the model was pre-run for 4 days to approach a steady state to stabilize the concentrations of unconstrained species, and results from the 5th day were extracted for analysis.

A series of sensitivity tests were conducted based on measurement data in spring, summer, and autumn, when Hong Kong experiences O_3 pollution (Fig. S1). The first series was performed to quantify the effect of changes in major precursor groups (i.e., CO, NO_x, VOCs, alkanes, alkenes, aromatics, and BVOCs) on in-situ O_3 production rates at TC. The sensitivity runs were conducted by rerunning the base models for 2014-2019 with constraints to target precursor group based on the 2013 measurement data, while the other parameters were fixed. The differences in in-situ O_3 production rates between the sensitivity and base runs can thus be ascribed to changes in the target precursor group. The second series was performed to examine the response of the O_3 formation regime to changes in major precursor groups (i.e., CO, NO_x, AVOCs (sub-grouped into alkanes, alkenes, and aromatics), and BVOCs). The sensitivity runs were conducted by rerunning the base models for 2013–2019 with a 10% reduction in the target precursor group, while the other parameters were fixed. The third series was performed to examine the effect of changes in BVOCs on the O_3-precursor (anthropogenic) relationship. The models for 2014-2019 in the second series were rerun with constraints to isoprene based on the 2013 measurement data, while the other parameters were fixed. The O_3-precursor relationship was evaluated by relative increment reactivity (RIR) (see SI for the calculation of RIR) (Cardelino and Chameides, 1995). A higher positive RIR value indicates that O_3 production is more sensitive to this precursor.

The O_3 isopleth diagram (i.e., the EKMA plot) was established to aid in the development of control strategies against O_3 pollution. A 1-day model input was designed based on average diurnal profile of major pollutants (e.g., NO, NO_2, HONO, SO_2, CO, CH_4, C_2–C_{10} NMVOCs) or parameters (e.g., temperature, RH, and JNO_2) during O_3 non-attainment days (i.e., MDA8 O_3 mixing ratio exceeds 75 ppbv) in 2019 (totally 25 cases). The input of NO_2 was obtained by adjusting the NO_2* data during O_3 non-attainment days at the TC station according to the NO_2*/NO_2 ratios measured during the top 10% of O_3 events at the same site by Xu et al. (2013) (See SI for details). O_3 was initialized according to observation data, and then its formation and chemistry were simulated freely with inputs of other relevant species in the following integration. A base run and a series of emission-reduction runs were performed by using X folds (0–1 fold with a bin precision of 0.025) inputs of NO_x and AVOCs. The model was initiated at 0:00 LT, and the integration had a step of 1 h and a duration of 24 h. The model-simulated O_3 concentrations under total 1600 (400 × 400) scenarios were extracted to describe the response of MDA8 O_3 concentration to decreases in NO_x and AVOCs concentration.

3. Results and discussion

3.1. Trends in O_3 and its precursors

Fig. 2 presents the trends in annual and seasonal mean O_3 concentrations, averaged for the 11 stations in Hong Kong, during 2013–2019. The mixing ratios of both hourly O_3 and MDA8 O_3 exhibited statistically significant ($p < 0.05$) increasing trends by 1.1 ± 0.9 ppbv/yr (slope ± 95% confidence interval) and 1.3 ± 1.0 ppbv/yr, respectively. The upward trend in Hong Kong is consistent with that in the PRD region with a rate of 1.1 ppbv/yr for MDA8 O_3 levels during the same period (Cao et al., 2024). The upward trend of O_3 was documented in all four seasons, with a large variance in the rates and statistical significance (Fig. 2b). For instance, the O_3 mixing ratio showed large and statistically significant increases in spring (1.5 ± 1.0 ppbv/yr), but relatively small increases in winter (0.5 ± 1.2 ppbv/yr) with low statistical significance (i.e., $p > 0.05$).

We further examined the impact of background O_3 and local chemistry on the observed O_3 trends (Fig. 3). The background O_3 levels were derived from measurements at a background site (Hok Tsui) in Hong Kong, and showed insignificant variations (0.2 ± 0.8 ppbv/yr; $p = 0.32$). The levels of background O_3 decreased in winter while increasing in the other three seasons (Fig. 3b). Thus, background O_3 contributed to the seasonal differences in O_3 trends but had a minor effect on the overall increasing O_3 trends. Similarly, the contributions of major air mass clusters and the background O_3 levels within each air mass cluster also showed insignificant variations (Fig. S2; see Wang et al. (2019) for the

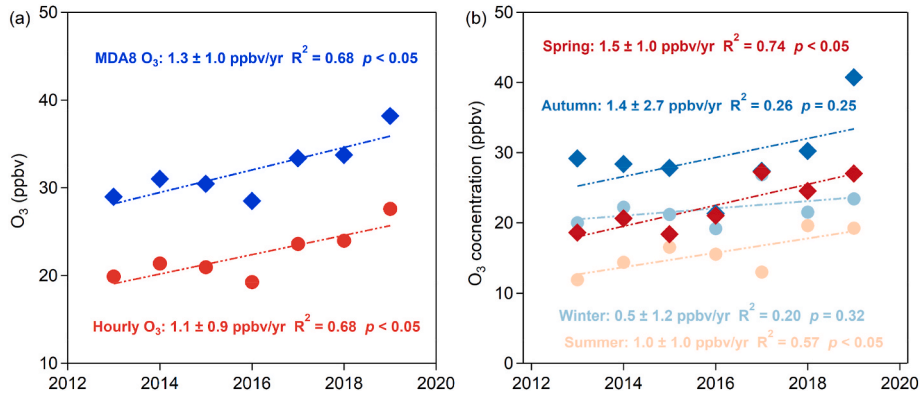

Fig. 2. Trends in (a) annual mean O_3 and maximum daily 8 h average (MDA8) O_3, and (b) seasonal mean O_3 recorded by 11 AQMSs in Hong Kong during 2013–2019. The fit lines indicate linear regressions with slopes (± 95% confidence intervals), R squares, and *p*-value annotated. Winter: December–February; Spring: March–May; Summer: June–August; Autumn: September–November.

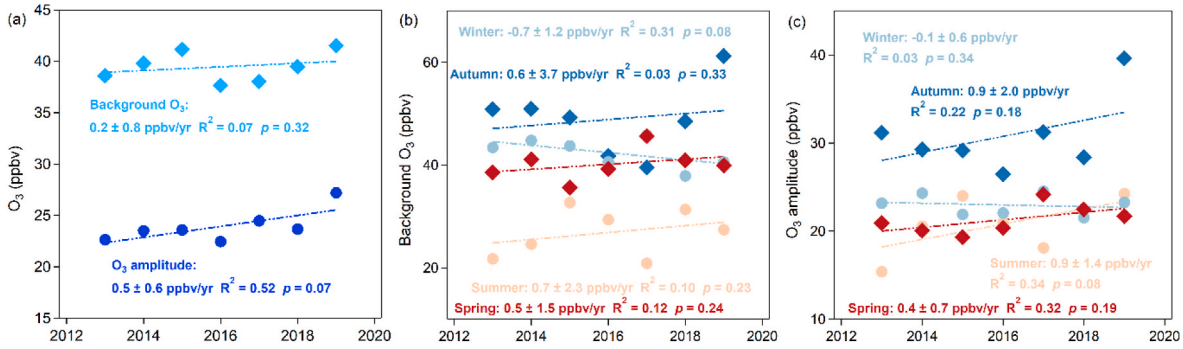

Fig. 3. Trends in (a) annual averages in background O_3 levels and O_3 amplitude, and seasonal averages in (b) background O_3 levels and (c) O_3 amplitude in Hong Kong during 2013–2019. The background O_3 levels were derived from measurements at Hok Tsui, a background site in Hong Kong. The fit lines indicate linear regressions with slopes (± 95% confidence intervals), R squares, and *p*-value annotated.

background O_3 levels within each air mass cluster). To examine the effect of local chemistry, we calculated the daily O_3 amplitude, which is the difference between the O_3 afternoon peak and the morning trough (see SI for the calculation). It should be pointed out that the O_3 amplitude is determined by not only local chemistry but also physical processes such as convection and deposition. The O_3 amplitude showed an increasing trend of 0.5 ± 0.6 ppbv/yr, and the rate of increase was more evident in seasons other than winter, likely suggesting increasing local O_3 production in recent years.

The trends in O_3 precursors were examined to find underlying causes for the increasing local O_3 production (Fig. 4). The data of CO and NO_x* were averaged for the 11 stations in Hong Kong, while VOCs were obtained from the TC station. These O_3 precursors were classified into two types, i.e., anthropogenic and biogenic precursors (see SI for the detailed descriptions). The anthropogenic precursors declined due to stringent control measures. Quantitatively, the concentrations of CO and NO_x* declined at rates of −20.2 ± 22.1 ppbv/yr and −4.0 ± 1.0 ppbv/yr, respectively, and the OH reactivity of AVOCs declined at a rate of −0.02 ± 0.03 s^{-1}/yr (see SI for the calculation of OH reactivity). This is also the case from a seasonal perspective, with a large variance in declining rates (Fig. S3 & Table S3). In winter, VOC levels showed the largest rate of decline, which should contribute to smaller increases in O_3

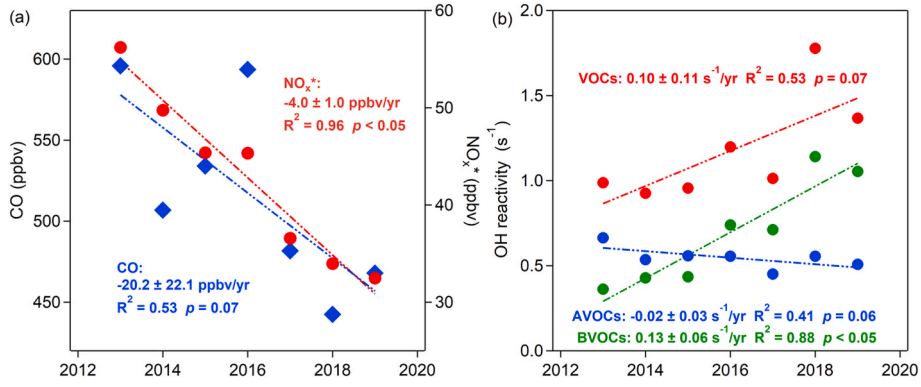

Fig. 4. (a) Annual mean concentrations of CO and NO_x* observed at available AQMSs (i.e., 4 for CO, and 9 for NO_x*) during 2013–2019. (b) Annual mean reactivity of selected VOC species at Tung Chung during 2013–2019. Only VOC species with data caption rate higher than 75% were selected for trend analysis (AVOCs: ethane, propane, *n*-butane, *i*-butane, propene, benzene, and toluene; BVOCs: isoprene).

concentrations compared to other seasons. We note that some species within alkanes (e.g., *n/i*-butane) and aromatics (e.g., xylenes and trimethyl benzene) showed increasing trends. The VOCs measurements at a roadside station in a busy commercial area (Mong Kok (MK), see Fig. 1 for its location) indicated drastic decreases in the concentrations of all the AVOC groups during the same period (Fig. S4). The smaller decreasing rates and increases in some VOCs at TC compared to MK may indicate influences of sources from the airport or outside Hong Kong.

In sharp contrast with the declining overall anthropogenic precursors, the OH reactivity of biogenic isoprene showed a surprisingly large increase rate of 0.13 ± 0.06 s^{-1}/yr (18% for a mean level of 0.70 s^{-1}). The satellite-derived column values of HCHO, a major oxidation product of biogenic isoprene, for the large areas of Hong Kong showed an increasing trend as well (Fig. 5) in 2019 compared to 2013. The increases in BVOCs should be dominantly driven by meteorological variations. From 2013 to 2019, the daytime average temperature in Hong Kong showed a significant upward trend at 0.14 ± 0.12 °C/yr, and the solar radiation slightly increased at a rate of 0.01 ± 0.12 MJ/m^2/yr (Fig. 6). Consistently, the ambient temperature in the adjacent PRD region also showed a significant upward trend at 0.19 ± 0.11 °C/yr (Fig. 6a; Guangdong Bureau of Statistics, 2013-2019). The higher temperature and stronger solar radiation would lead to higher leaf temperature and stronger photosynthetically active radiation, and then lead to more intense BVOCs emission (Chang et al., 2009; Sabillón and Cremades, 2001).

3.2. Impact of changes in BVOCs and other precursors on O_3 production

Given the large increase in BVOCs, the increases in locally-produced O_3 are unsurprising. In addition, we note that the concentration of O_x* (=O_3 + NO_2*) and MDA8 O_x* exhibited slightly decreasing trends (Fig. S5), indicating that the reduced NO titration effect should also contribute to the increases in locally-produced O_3 in Hong Kong. In this section, a detailed MCM box model was employed to quantify the effect resulting from changes in major O_3 precursors at the TC station.

The model-calculated rates of in-situ O_3 production at TC showed a significant upward trend at 1.33 ± 0.67 ppbv/h/yr, which is consistent with observations (Fig. 7a). Fig. 7b and S6 present the effect of changes in major precursor groups (i.e., CO, NO_x, and VOCs) on in-situ O_3 production rates at TC. The increasing local O_3 production was dominated by changes in precursors, while the role of other factors (e.g., increasing reaction rates due to elevated temperature) was relatively small. Based on slopes from linear regression analysis, changes in precursors explained 86% of the increases in local O_3 production (i.e., 0.74 ppbv/h/yr), while other factors explained the remaining 14% (i.e., 0.12 ppbv/h/yr). Within major O_3 precursor groups, decreases in CO slightly reduced the O_3 production by −0.03 ppbv/h/yr (i.e., −3%), while changes in NO_x and VOCs increased O_3 production by 0.41 ppbv/h/yr (i.e., 31%) and 0.45 ppbv/h/yr (i.e., 34%), respectively. Thus, the increasing local O_3 production in Hong Kong was mainly driven by changes in VOCs and NO_x. Seasonally, decreases in NO_x dominated the increasing local O_3 production in spring (by 0.45 ppbv/h/yr or 46%), when the levels of NO_x* concentration showed the largest rate of decline (Fig. S3) and the levels of O_3 concentration showed the largest rate of increase (Fig. 2b). This is attributed to the reduced NO titration effect, which would enhance O_3 production by increasing radical levels (Fig. S7). In contrast, increases in VOCs dominated the increasing local O_3 production in summer (by 0.63 ppbv/h/yr or 38%) and autumn (by 0.47 ppbv/h/yr or 35%). Similarly, increases in VOCs would promote radical cycling (Fig. S7) and thus enhance O_3 production.

We further examined the role of major VOC groups, i.e., BVOCs and AVOCs, and AVOCs were sub-grouped into alkanes, alkenes, and aromatics (Fig. 7b). Changes in AVOCs overall increased O_3 production (by 0.14 ppbv/h/yr or 10%), but the effect varied among subgroups. Specifically, decreases in alkenes slightly reduced O_3 production (by −0.01 ppbv/h/yr or −1%), while changes in alkanes and aromatics enhanced O_3 production (by 0.11 ppbv/h/yr or 8% for alkanes; by 0.04 ppbv/h/yr or 3% for aromatics). In comparison, the effect of BVOCs on O_3 production is much larger. Annually, increasing BVOCs enhanced O_3 production by 0.31 ppbv/h/yr (i.e., 23%), which is comparable to the effect of reduced NO_x. Seasonally, the effect of BVOCs on O_3 production was the most obvious in summer (by 0.44 ppbv/h/yr or 27%), when the levels of isoprene showed the largest rate of increase (0.08 ± 0.04 ppbv/yr) (Table S3). These results are a lower limit of BVOCs effect on O_3 production, since some BVOC species (e.g., monoterpene and sesquiterpene) were not considered in this study due to the lack of available measurement data.

Taken together, the increasing photochemical O_3 production at TC in Hong Kong in recent years was dominated by changes in O_3 precursors, especially by the reduction in NO_x and the increases in biogenic isoprene. We note different trends in local O_3 production at TC during 2002-2013 (decline by −0.20 ± 0.14 ppbv/h/yr) (Xue et al., 2014) and in 2013–2019 (increase by 1.33 ± 0.67 ppbv/h/yr). During 2002-2013, the significant decline in aromatics overcame the reduced NO titration effect and led to decreasing O_3 production (Xue et al., 2014). In contrast, during 2013–2019, the small variation of aromatics was insufficient to negate the effect of reduced NO_x (and increased isoprene) and thus led to increasing O_3 production.

3.3. Impact of increased BVOCs on O_3-precursor relationships and control efforts

Increased BVOCs not only enhanced local O_3 production but also affected the O_3-precursor (anthropogenic) relationships. As shown in Fig. 8, increased BVOCs increased the sensitivity of O_3 production to NO_x, but decreased the sensitivity of O_3 production to AVOCs and CO. During 2013–2019, the RIRs for NO_x, CO, and AVOCs changed by 0.12 ± 0.03 yr^{-1}, −0.02 ± 0.01 yr^{-1}, and −0.03 ± 0.01 yr^{-1}, respectively. In comparison, if the level of BVOCs had remained unchanged since 2013 (solely with changes in anthropogenic precursors), the RIRs for NO_x, CO, and AVOCs would have changed by 0.10 ± 0.03 yr^{-1}, −0.02 ± 0.01 yr^{-1}, and −0.02 ± 0.01 yr^{-1}, respectively. Within major AVOC groups, the increased BVOCs exerted the largest effect on the RIRs for alkenes (Fig. 8b). The effect of BVOCs on O_3-precursor (anthropogenic)

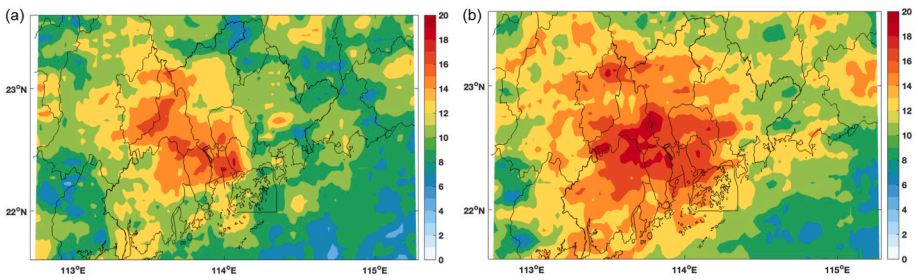

Fig. 5. Spatial distribution of vertical HCHO column concentrations (in 10^{15} molecules/cm^3) in Hong Kong and the adjacent Pearl River Delta region in the O_3-peak autumn season in (a) 2013 and (b) 2019. The data of the vertical HCHO column were retrieved from Ozone Monitoring Instrument (https://h2co.aeronomie.be/).

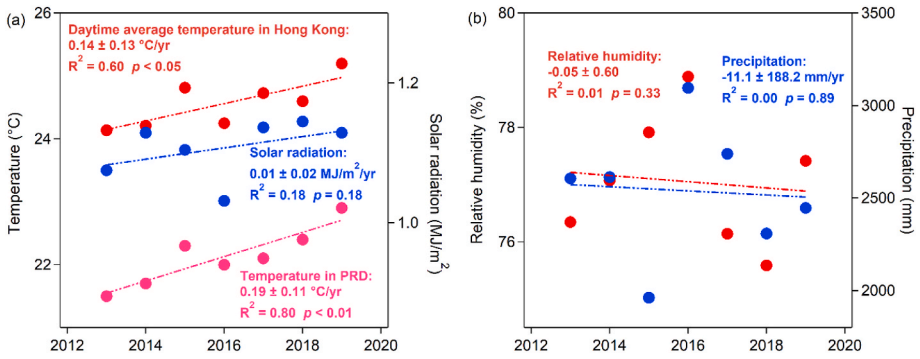

Fig. 6. Trends in major meteorological parameters in Hong Kong and the Pearl River Delta region during 2013–2019. The meteorological data in Hong Kong were obtained from King's Park (https://www.hko.gov.hk/sc/index.html). The data on the annual average temperature in the Pearl River Delta region were derived from the Guangdong Statistical Yearbook (http://stats.gd.gov.cn/gdtjnj/index.html). The fit lines indicate linear regressions with slopes (± 95% confidence intervals), R squares, and *p*-value annotated.

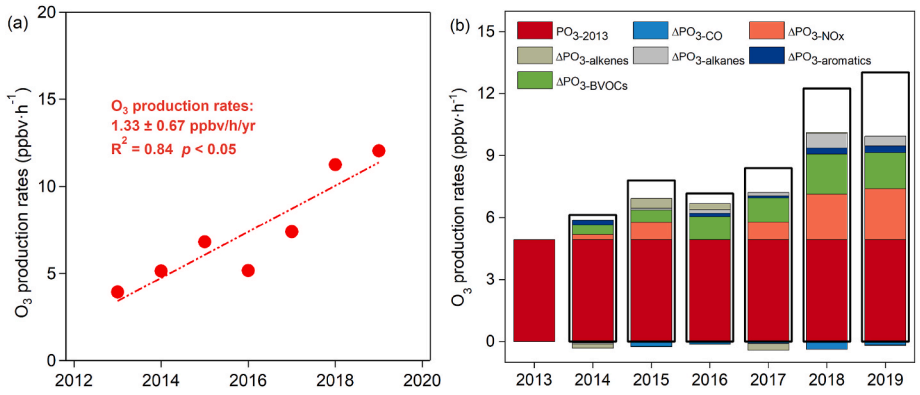

Fig. 7. (a) Trend in model-calculated midday (9:00–15:00 LT) net O_3 production rates at Tung Chung during 2013–2019 (b) Effect of changes in major O_3 precursor groups (i.e., NO_x, BVOCs, alkanes, alkenes, and aromatics) on midday net O_3 production rates (average results from spring, summer, and autumn). The black open bar indicates the net rates of O_3 production calculated under base scenarios during 2014–2019, the red solid bar indicates the net rates of O_3 production calculated under the base scenario in 2013, and the solid bar in other colors indicates the net rates of O_3 production resulting from changes in target O_3 precursor group (relative to 2013).

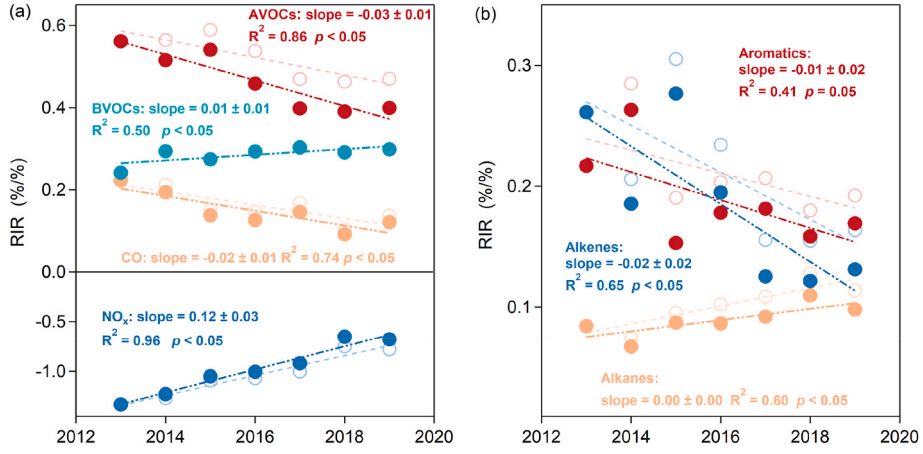

Fig. 8. Trends in model-calculated relative incremental reactivity (RIR) for (a) major O_3 precursor groups (i.e., CO, NO_x, AVOCs, and BVOCs) and (b) major AVOC groups (i.e., alkanes, alkenes, and aromatics) at Tung Chung. The solid circles indicate the true trends from the base scenarios, and the open circles show the "trends" if the BVOCs remained the same as in 2013. The fit lines indicate linear regressions with slopes (± 95% confidence intervals), R squares, and *p*-value annotated.

relationships was determined by the role of target precursors in O_3 production. Same to AVOCs and CO, the degradation of BVOCs and their products produces HO_2 and RO_2 to oxidize NO to NO_2. Under high NO_x conditions (which is the case for Hong Kong), increased BVOCs would efficiently promote radical cycling and enhance radical level (Fig. S8). This would make O_3 production less sensitive to the intensity of the "RO_x (=OH + HO_2 + RO_2) radical cycle" (i.e., to AVOCs and CO) and more sensitive to the intensity of the "NO_x cycle" (i.e., NO_x).

Although the O_3-precursor relationships were affected by the increasing BVOCs, the O_3 formation remained in NO_x-saturated and VOC-limited regimes at TC (Figs. 8 and 9). Decreases in AVOCs would effectively alleviate O_3 pollution during a short-time period, while decreases in NO_x would aggravate O_3 pollution. For the attainment of MDA8 O_3 concentration (i.e., <75 ppbv or 160 $\mu g/m^3$) at the TC site, the AVOCs concentration would need to be reduced by 35% (Fig. 9b). However, it is challenging to further reduce MDA8 O_3 concentration to the World Health Organization (WHO)'s recommended guideline (100 $\mu g/m^3$ or 47 ppbv) (WHO, 2021) solely based on AVOCs control - the MDA8 O_3 could only be reduced to 50 ppbv even with 100% AVOCs reduction.

For the NO_x control pathway, taking the BVOCs into account, a deep cut in NO_x emission would be needed to achieve the WHO guideline at the site, which aims to reduce NO_x emission large enough to eliminate the NO titration effect and shift the O_3 formation regime from VOC-

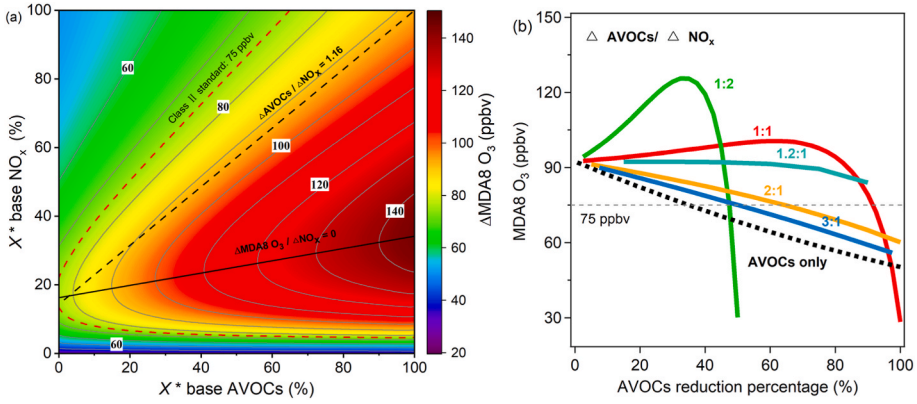

Fig. 9. (a) Contour plots of the model-simulated MDA8 O_3 concentrations as a function of the base concentrations of NO_x and AVOCs during O_3 non-attainment days (i.e., MDA8 O_3 mixing ratio exceeded 75 ppbv). The black solid line represents the boundary between the VOC-limited and mixed-limited ($\triangle$MDA8 $O_3/\triangle NO_x$ = 0) O_3 formation regime. The black dashed line represents the fitting line for a base case with an $\triangle$AVOCs/$\triangle NO_x$ reduction ratio = 1.2 [= percentage change in concentration (ppbv)/percentage change in concentration (ppbv)], which exerts nearly zero effect on O_3 production (whereas the combined effects of an $\triangle$AVOCs/$\triangle NO_x$ reduction ratio >1.2 (i.e., above the fitting line) would lead to decreased O_3 production). (b) The model-simulated MDA8 O_3 change under different $\triangle$AVOCs/$\triangle NO_x$ reduction ratios.

limited to mixed-limited and eventually to NO_x-limited condition. However, to reach the mixed-limited regime, the NO_x concentration at TC would have to be reduced by −66% from the 2019 level (see the black solid line in Figs. 9a), and 99% NO_x reductions would be needed to meet the WHO guideline. Such a large decrease in NO_x reduction poses a huge challenge for the existing de-NO_x technologies. Thus, a transformation of current energy and transportation is necessary, such as rapid uptake of renewable energy and electrifying transportation.

For TC, in the short term, a combined AVOCs and NO_x control strategy - with $\triangle$AVOCs/$\triangle NO_x$ reduction ratio larger than 1.2 (see the black dashed line in Fig. 9a) - can be taken to reduce MDA8 O_3 to below the current standard (75 ppbv) and to reduce NO_2 pollution in the same time.

We acknowledge that the above results are derived from the detailed chemical measurements obtained at one site (TC). Similar VOCs measurement and modeling studies in other areas of Hong Kong would be needed in order to obtain a more robust conclusion on the O_3-precursor relationship and the precursor control strategy for the whole territory of Hong Kong. Nonetheless, the long-term VOCs measurement at TC and the model analysis provide valuable insights into the local O_3 chemistry and O_3-precursor control.

3.4. Implications and conclusions

The continuous observations of O_3 and its precursors in Hong Kong provide strong evidence for the increasing BVOCs emission in recent years. The increase in BVOCs is believed to be driven by meteorological conditions, especially by the elevated surface temperature. As shown in Fig. 5, the vertical HCHO column concentrations in the O_3-peak autumn season showed increasing trends in the adjacent PRD region in 2019 compared to 2013, likely owing to the increased biogenic isoprene emissions under the warming temperature (Fig. 6a). The increased biogenic emissions may have contributed to the increasing O_3 concentrations in the PRD region (Cao et al., 2024). Ren et al. (2022) also found that the HCHO column concentrations showed increasing trends (by 1%/yr) in Eastern China during 2013–2019, and the interannual variability of the HCHO column was highly consistent with that of surface temperature. Thus, weather-induced BVOCs enhancement should occur at a large regional scale rather than just at the TC site. In view of accelerating climate warming (IPCC, 2021) and urban greening (Cao et al., 2022), the impact of BVOCs should be considered in formulating control policies for the anthropogenic precursors of O_3. For cities like Hong Kong, where ozone formation is mainly controlled by VOCs, increasing BVOCs emission will limit the potential of AVOCs control in meeting a more stringent O_3 standard. Nonetheless, in the short term, AVOC control will help to reduce the O_3 levels to comply with the current standard; in the long run, a drastic cut in NO_x emission will be needed, which requires transformative changes in current energy and transportation sectors, such as rapid and large-scale adoptions of renewable energy and green transportation.

CRediT authorship contribution statement

Yingnan Zhang: Data curation, Methodology, Formal analysis, Writing – original draft. **Jianing Dai:** Data curation, Methodology, Writing – review & editing. **Qinyi Li:** Methodology, Writing – review & editing. **Tianshu Chen:** Methodology. **Jiangshan Mu:** Methodology. **Guy Brasseur:** Writing – review & editing. **Tao Wang:** Supervision, Resources, Funding acquisition, Project administration, Writing – review & editing. **Likun Xue:** Supervision, Resources, Funding acquisition, Project administration, Writing – review & editing.

Declaration of competing interest

The authors declare that they have no known competing financial interests or personal relationships that could have appeared to influence the work reported in this paper.

Data availability

Data will be made available on request.

Acknowledgements

We thank the Hong Kong Environmental Protection Department for providing the air-quality data, Hong Kong Observatory for providing the meteorological data, Glenn Wolfe for providing the platform of F0AM, and the University of York for providing the Master Chemical Mechanism (version 3.3.1). This work was sponsored by the National Natural Science Foundation of China (42061160478 and 41922051 to LX), the Hong Kong Research Grants Council (T24-504/17-N to TW), and the Hong Kong Environmental Protection Department (Tender Ref: 20-00901 to TW). The opinions expressed in this paper are those of the authors and do not necessarily reflect the views or policies of the Hong Kong Special Administrative Region, nor does mention of trade names or commercial products constitute an endorsement or recommendation of their use.

Appendix A. Supplementary data

Supplementary data to this article can be found online at https://doi.org/10.1016/j.atmosenv.2023.119917.

References

Agathokleous, E., Feng, Z., Oksanen, E., Sicard, P., Wang, Q., Saitanis, C., Araminiene, V., Blande, J., Hayes, F., Calatayud, V., Domingos, M., Veresoglou, S., Peñuelas, J., Wardle, D., Marco, A., Li, Z., Harmens, H., Yuan, X., Vitale, M., Paoletti, E., 2020.

Ozone affects plant, insect, and soil microbial communities: a threat to terrestrial ecosystems and biodiversity. Sci. Adv. 6.
Cao, J., Situ, S., Hao, Y., Xie, S., Li, L., 2022. Enhanced summertime ozone and SOA from biogenic volatile organic compound (BVOC) emissions due to vegetation biomass variability during 1981–2018 in China. Atmos. Chem. Phys. 22, 2351–2364.
Cardelino, C., Chameides, W., 1995. An observation-based model for analyzing ozone precursor relationships in the urban atmosphere. J. Air Waste Manag. Assoc. 45, 161–180.
Chang, K., Yu, J., Chen, T., Lin, Y., 2009. Estimating Taiwan biogenic VOC emission: leaf energy balance consideration. Atmos. Environ. 43, 5092–5100.
Cao, T., Wang, H., Li, L., Lu, X., Liu, Y., Fan, S., in-press. Fast spreading of surface ozone in both temporal and spatial scale in pearl river delta. J. Environ. Sci. 137, 540-552.
EPD, 2013-2019. Air Quality in Hong Kong.
Fleming, Z., Doherty, R., von Schneidemesser, E., Malley, C., Cooper, O., Pinto, J., Colette, A., Xu, X., Simpson, D., Schultz, M., Lefohn, A., Hamad, S., Moolla, R., Solberg, S., Feng, Z., 2018. Tropospheric ozone assessment report: present-day ozone distribution and trends relevant to human health. Elementa: Elem. Sci. Anth. 6, 12–52.
Gaudel, A., Cooper, O., Ancellet, G., Barret, B., Boynard, A., Burrows, J., Clerbaux, C., Coheur, P., Cuesta, J., Cuevas, E., Doniki, S., Dufour, G., Ebojie, F., Foret, G., Garcia, O., Granados-Muñoz, M., Hannigan, J., Hase, F., Hassler, B., Huang, G., Hurtmans, D., Jaffe, D., Jones, N., Kalabokas, P., Kerridge, B., Kulawik, S., Latter, B., Leblanc, T., Le Flochmoën, E., Lin, W., Liu, J., Liu, X., Mahieu, E., McClure-Begley, A., Neu, J., Osman, M., Palm, M., Petetin, H., Petropavlovskikh, I., Querel, R., Rahpoe, N., Rozanov, A., Schultz, M., Schwab, J., Siddans, R., Smale, D., Steinbacher, M., Tanimoto, H., Tarasick, D., Thouret, V., Thompson, A., Trickl, T., Weatherhead, E., Wespes, C., Worden, H., Vigouroux, C., Xu, X., Zeng, G., Ziemke, J., 2018. Tropospheric ozone assessment report: present-day distribution and trends of tropospheric ozone relevant to climate and global atmospheric chemistry model evaluation. Elementa: Elem. Sci. Anth. 6, 39–96.
Guangdong Bureau of Statistics, 2013-2019. Guangdong Statistical Yearbooks.
Guo, H., Ling, Z., Cheng, H., Simpson, I., Lyu, X., Wang, X., Shao, M., Lu, H., Ayoko, G., Zhang, Y., Saunders, S., Lam, S., Wang, J., Blake, D., 2017. Tropospheric volatile organic compounds in China. Science of The Total Environment 574, 1021–1043.
IPCC, 2021. Climate Change 2021: The Physical Science Basis. Contribution of Working Group I to the Sixth Assessment Report of the Intergovernmental Panel on Climate Change 2391. Cambridge University Press, Cambridge, United Kingdom and New York, NY, USA.
Jenkin, M., Saunders, S., Wagner, V., Pilling, M., 2003. Protocol for the development of the master chemical mechanism, MCM v3 (Part B): tropospheric degradation of aromatic volatile organic compounds. Atmos. Chem. Phys. 3, 181–193.
Jenkin, M., Young, J., Rickard, A., 2015. The MCM v3.3.1 degradation scheme for isoprene. Atmos. Chem. Phys. 15, 11433–11459.
Lefohn, A., Malley, C., Smith, L., Wells, B., Hazucha, M., Simon, H., Naik, V., Mills, G., Schultz, M., Paoletti, E., De Marco, A., Xu, X., Zhang, L., Wang, T., Neufeld, H., Musselman, R., Tarasick, D., Brauer, M., Feng, Z., Tang, H., Kobayashi, K., Sicard, P., Solberg, S., Gerosa, G., 2018. Tropospheric ozone assessment report: global ozone metrics for climate change, human health, and crop/ecosystem research. Elementa: Elem. Sci. Anth. 6, 28–66.
Mills, G., Pleijel, H., Malley, C., Sinha, B., Cooper, O., Schultz, M., Neufeld, H., Simpson, D., Sharps, K., Feng, Z., Gerosa, G., Harmens, H., Kobayashi, K., Saxena, P., Paoletti, E., Sinha, V., Xu, X., 2018. Tropospheric ozone assessment report: present-day tropospheric ozone distribution and trends relevant to vegetation. Elementa: Elem. Sci. Anth. 6, 47–92.
Ren, J., Guo, F., Xie, S., 2022. Diagnosing ozone-NOx-VOC sensitivity and revealing causes of ozone increases in China based on 2013–2021 satellite retrievals. Atmos. Chem. Phys. 22, 15035–15047.
Sabillón, D., Cremades, L., 2001. Diurnal and seasonal variation of monoterpene emission rates for two typical mediterranean species (pinus pinea and quercus ilex) from field measurements—relationship with temperature and PAR. Atmos. Environ. 35, 4419–4431.
Saunders, S., Jenkin, M., Derwent, R., Pilling, M., 2003. Protocol for the development of the master chemical mechanism, MCM v3 (Part A): tropospheric degradation of non-aromatic volatile organic compounds. Atmos. Chem. Phys. 3, 161–180.
Sun, L., Xue, L., Wang, T., Gao, J., Ding, A., Cooper, O., Lin, M., Xu, P., Wang, Z., Wang, X., Wen, L., Zhu, Y., Chen, T., Yang, L., Wang, Y., Chen, J., Wang, W., 2016. Significant increase of summertime ozone at mount tai in central eastern China. Atmos. Chem. Phys. 16, 10637–10650.
Sun, L., Xue, L., Wang, Y., Li, L., Lin, J., Ni, R., Yan, Y., Chen, L., Li, J., Zhang, Q., Wang, W., 2019. Impacts of meteorology and emissions on summertime surface ozone increases over central eastern China between 2003 and 2015. Atmos. Chem. Phys. 19, 1455–1469.
Wang, T., Dai, J., Lam, K., Poon, C., Brasseur, G., 2019. Twenty-Five years of lower tropospheric ozone observations in tropical East Asia: the influence of emissions and weather patterns. Geophys. Res. Lett. 46, 11463–11470.
Wang, T., Xue, L., Brimblecombe, P., Lam, Y., Li, L., Zhang, L., 2017a. Ozone pollution in China: a review of concentrations, meteorological influences, chemical precursors, and effects. Sci. Total Environ. 575, 1582–1596.
Wang, T., Xue, L., Feng, Z., Dai, J., Zhang, Y., Tan, Y., 2022. Ground-level ozone pollution in China: a synthesis of recent findings on influencing factors and impacts. Environ. Res. Lett. 17, 063003.
Wang, Y., Wang, H., Guo, H., Lyu, X., Cheng, H., Ling, Z., Louie, P.K.K., Simpson, I.J., Meinardi, S., Blake, D.R., 2017b. Long-term O_3–precursor relationships in Hong Kong: field observation and model simulation. Atmos. Chem. Phys. 17, 10919–10935.
WHO, 2021. WHO Global Air Quality Guidelines: Particulate Matter ($PM_{2.5}$ and PM_{10}), Ozone, Nitrogen Dioxide, Sulfur Dioxide and Carbon Monoxide.
Wolfe, G.M., Marvin, M.R., Roberts, S.J., Travis, K.R., Liao, J., 2016. The framework for 0-D atmospheric modeling (F0AM) v3.1. Geosci. Model Dev. (GMD) 9, 3309–3319.
Xia, M., Wang, T., Wang, Z., Chen, Y., Peng, X., Huo, Y., Wang, W., Yuan, Q., Jiang, Y., Guo, H., Lau, C., Leung, K., Yu, A., Lee, S., 2022. Pollution-derived Br_2 boosts oxidation power of the coastal atmosphere. Environ. Sci. amp; Technol. 56, 12055–12065.
Xu, Z., Wang, T., Wu, J., Xue, L., Chan, J., Zha, Q., Zhou, S., Louie, P.K., Luk, C., 2015. Nitrous acid (HONO) in a polluted subtropical atmosphere: seasonal variability, direct vehicle emissions and heterogeneous production at ground surface. Atmos. Environ. 106, 100–109.
Xu, Z., Wang, T., Xue, L., Louie, P., Luk, C., Gao, J., Wang, S., Chai, F., Wang, W., 2013. Evaluating the uncertainties of thermal catalytic conversion in measuring atmospheric nitrogen dioxide at four differently polluted sites in China. Atmos. Environ. 76, 221–226.
Xue, L., Wang, T., Louie, P., Luk, C., Blake, D., Xu, Z., 2014. Increasing external effects negate local efforts to control ozone air pollution: a case study of Hong Kong and implications for other Chinese cities. Environ. Sci. amp; Technol. 48, 10769–10775.
Zeren, Y., Guo, H., Lyu, X., Zhou, B., Liu, X., Yang, L., Yuan, Z., Wang, Y., 2022. Remarkable spring increase overwhelmed hard-earned autumn decrease in ozone pollution from 2005 to 2017 at a suburban site in Hong Kong, South China. Sci. Total Environ. 831, 154788.
Zhang, J., Wei, Y., Fang, Z., 2019. Ozone pollution: a major health hazard worldwide. Front. Immunol. 10.
Zhang, Y., Xue, L., Carter, W., Pei, C., Chen, T., Mu, J., Wang, Y., Zhang, Q., Wang, W., 2021a. Development of ozone reactivity scales for volatile organic compounds in a Chinese megacity. Atmos. Chem. Phys. 21, 11053–11068.
Zhang, Y., Xue, L., Li, H., Chen, T., Mu, J., Dong, C., Sun, L., Liu, H., Zhao, Y., Wu, D., Wang, X., Wang, W., 2021b. Source apportionment of regional ozone pollution observed at Mount Tai, North China: application of lagrangian photochemical trajectory model and implications for control policy. J. Geophys. Res. Atmos. 126, e2020JD033519.